

An experimental study of Roman dropshaft hydraulics

Une étude expérimentale de l'hydraulique des puits de rupture romains

H. CHANSON, MIAHR, *Senior Lecturer, Fluid Mechanics, Hydraulics and Environmental Engineering, Department of Civil Engineering, The University of Queensland, Brisbane QLD 4072, Australia, Email: h.chanson@mailbox.uq.edu.au*

Abstract

In Roman aqueducts, series of vertical dropshafts were used to dissipate the kinetic energy of the flow: i.e., the dropshaft cascades. A re-analysis of Roman dropshaft hydraulics is conducted with physical model tests. Three basic flow patterns are observed. The results demonstrate that the vertical dropshafts could be very efficient energy dissipators and re-oxygenation structures, under appropriate flow conditions. The optimum operation of Roman dropshaft is discussed and an analytical model is developed to predict these conditions. Further the performances of aqueduct dropshafts are compared with modern dropshaft designs, and the operation of dropshaft cascades is discussed. Additional material is available upon request.

Résumé

Certains aqueducs romains étaient équipés de cascades de puits de rupture, conçues pour briser l'énergie cinétique de l'écoulement. On a conduit une série de tests sur modèles physiques pour ré-analyser l'hydraulique des puits de rupture romains. Les résultats démontrent trois régimes d'écoulement. Dans des conditions optimales, les puits de rupture sont des systèmes de perte de charge très efficaces. Ces conditions optimales ont été déterminées avec des modèles physiques et analytiques. Les performances des puits romains sont aussi comparées avec celles de puits modernes, et on discute aussi de l'opération des cascades de puits. Sur demande, l'auteur peut fournir de plus amples informations.

Introduction

The hydraulic expertise of the Romans has contributed significantly to the advance of science and engineering in the Antiquity and up to the end of the Middle Age. The aqueducts at Rome, in France and North Africa left magnificent ruins for example (e.g. ASHBY 1925, RAKOB 1974). Their construction was an enormous task conducted by the army (e.g. FEVRIER 1991). The total cost and duration of the works were functions of the difficulties: i.e., tunnels, bridges, arcades, raised foundation, siphons. Completion of the works could take from 3 years to over 15 years. The cost ranged between 23 to 69 millions of US\$ per kilometre¹. The aqueducts were designed for small flow rates (0.2 to 2 m³/s maximum) with flat longitudinal slopes: i.e., 1 to 3 m/km in average (e.g. HODGE 1992). Short sections with steep gradients up to 78% were sometimes introduced (CHANSON 2000). Field observations suggest primarily three designs: steep "smooth" chutes, stepped channel and the dropshaft cascade (Fig. 1). The stepped chute design was common also with dam spillways². The use of dropshaft³ and dropshaft cascade along the main branch of aqueducts was a specific engineering feature of a new aqueduct. From a sole hydraulic perspective, the dropshafts might have been used for: (1) a vertical drop in invert elevation, (2) kinetic energy dissipation, and (3) flow aeration. In the first application, a dropshaft allows the connection between two flat conduits, located at different elevations, along a very short distance: i.e., the shaft length L . The second application is the dissipation of the kinetic energy of the flow. Such a design is still used

today (e.g. JAIN and KENNEDY 1983, APELT 1984, RAJARATNAM et al. 1997) although it must be optimised for optimum operation, and to prevent scour and erosion. A third application is the aeration of the flow: e.g., re-oxygenation (e.g. ERVINE and AHMED 1982).

Table 1 summarises the main characteristics of well-documented Roman aqueduct dropshaft and dropshaft cascades. Although their intended purpose(s) is today poorly understood, the cascades were used in steep topography predominantly: e.g., at Recret, Vaugneray and Grézieu-la-Varenne, Yzeron aqueduct (Lyon, Fr.); at Montjeu, Autun aqueduct (Fr.) (Table 1). Most Roman dropshafts were designed with the outflow channel located on the opposite wall to the inflow (Fig. 1, 2A and 3A). An unusual de-

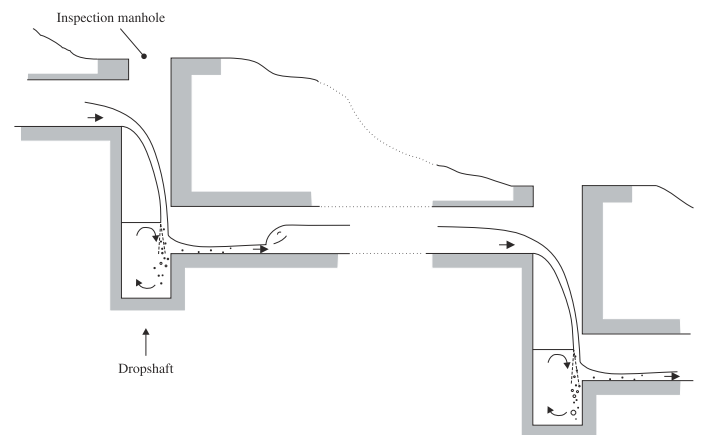


Fig. 1 Sketch of a dropshaft cascade in Roman aqueduct

Revision received July 26, 2000. Open for discussion till August 31, 2002.

1. That is, 1 to 3 millions of sesterces per km (LEVEAU 1991) converted into 1999 US\$ using the silver weight of the sesterce as a reference.
2. The oldest stepped spillway was built around BC 1,300 in Greece (CHANSON 1997) and several stepped chutes were used prior to the Roman era (e.g. CHANSON 1995, pp. 23-37). Roman engineers built also several significant stepped spillways: e.g., Kasserine dam, Tunisia AD 100?, Oued Guergour dam, Tunisia AD 100?.
3. "dropshaft" in English, "puit de rupture" in French, "Tosbecken" in German, "pozo resalto" in Spanish.

Table 1: Dropshaft cascades in Roman aqueducts

Steep Section (1)	Ref. (2)	Geometry (3)	Flow conditions (4)	Remarks (5)
Dougga aqueduct Oued Melah	[Ca]	B ~ 3.3 m b ~ 0.35 m (tunnel)	$\Delta H \sim 4$ to 5 m	Located downstream of 200-m long bridge, upstream of tunnel..
Vaugneray, Yzeron aqueduct Puit du Bourg	[Co1]	Rectangular dropshaft : h = 2.55 m, b = 0.4 m, B = 1.14 m, L = 1.9 m	$\Delta H = 21.9$ m $d_c \approx 0.24$ m (?) d/s flow conditions : d ~ 0.35 m, V ~ 1.33 m/s	Vaugneray branch of Yzeron aqueduct.
Recret/Grézieu-la-Varenne, Yzeron aqueduct	[Co1]	Rectangular dropshafts	$\Delta H = 38$ m	Main branch of Yzeron aqueduct.
Puit Gouttenoire		Square dropshaft : h = 2.55 m, b = 0.55 m, B = L = 1.18 m, P = 1.12 m	$d_c \approx 0.197$ m	
Puit-en-bas		Rectangular dropshaft : h = 2.5 m, b = 0.55 m, B = L = 1.17 m, D = 1.26 m, P = 1.35 m	d/s flow conditions : d ~ 0.15 m, V ~ 1.9 m/s	
Chabet Ilelouine, Cherchell aqueduct	[LP]		$\Delta H = 12.28$ m	4 series of steep chutes followed by circular dropshaft.
Puit amont		Circular dropshaft : h \approx 0.77 m, b \approx 0.94 m, $\phi = L = 2.03$ m, P > 1.75 m	Supercritical upstream flow : V ~ 8 m/s	Located downstream of steep smooth chute.
Gunugu aqueduct Moulin Romain	[LP]	Circular dropshaft : h ~ 3.5 to 4 m, b \approx 0.38 m, $\phi = L = 0.80$ m	$\Delta H = 20$ m	Upstream channel : 0.86-m wide.
Ruscade aqueduct	[Ve]	Circular dropshafts		
Beaulieu aqueduct Puit d'Olivari	[CQ]	Dropshaft : h = 6.2 m, b ~ 0.45 to 0.6 m	$\Delta H = 37$ m	Combination of steep chutes and dropshafts. Rectangular or circular ? 147-m between dropshaft.
Puit du Château		Dropshaft : h ~ 8 m		Rectangular or circular ? 167-m between dropshaft.
Brisecou Forest, Montjeu aq- ueduct	[CQ, PR]	Rectangular dropshaft : h = 4.4 m, b = 0.8 m, B = 3.0 m, L = 2.4 m, D = 1.57 m, P > 0.8 m 9 dropshafts (h = 4.4 m) 15 dropshafts (h = 4.4 m)	$\Delta H \sim 140$ m x ~ 770 m	A series of 24 dropshafts (possible combina- tion with steep chutes). 15 to 30-m between dropshaft. 50 to 120-m between dropshaft.
Cuicul aqueduct Grand thermes distribution line	[Al]	Circular (?) dropshafts: h~1 to 0.4 m, b \approx 0.45 m, $\phi = L = 0.80$ m	$\Delta H \sim 3$ m x ~ 85 m	Series of 4 dropshafts on an urban distribu- tion line.
Köln aqueduct Mechernich-Lessenich	[Gr]	Rectangular dropshaft : h = 0.35 m, b = 0.7 to 0.75 m, B = 0.9 m, L = 1.185 m, P = 0.2 m		[Gr, p. 97] One dropshaft installed along a steep section ($\Delta H \sim 84$ m, $\theta \sim 2.6^\circ$).
Valdepuentes aqueduct (Aqua Vetus), Cordoba	[Lop, Vi1, Vi2]			Several dropshafts and dropshaft cascades.
		One (?) dropshaft	$\Delta H = 3$ m	Hornillo
		Dropshaft cascade : 34 dropshafts	$\Delta H \sim 120$ m x ~ 400 m	Cerro de los Pinos. Upstream of Valdepuentes bridge. Three unusual 90-degree bend shafts: <i>spiramina</i> . Shaft equipped with steps sculpted inside (h ~ 0.5 m).
		Pozo No. 11: circular dropshaft: h \approx 2.9 m, b \approx 0.6 m, $\phi = L = 0.61$ m, P = 0.76 m u/s slope : $\theta \sim 5\%$ d/s slope : $\theta \sim 5\%$		
		Pozo No. 21: circular dropshaft: h \approx 3.1 m, b \approx 0.5 m, $\phi = L = 0.55$ m, P = 0.9 m		90-degree bend shaft equipped with steps sculpted inside (h ~ 0.6 m).

Dropshaft cascade: 7 dropshafts	$\Delta H \sim 200$ m (?)	Madinat-al-Zhara. Downstream of Valdepuentes bridge.
Dropshaft cascade (?) : at least two dropshafts	$\Delta H \sim 20$ m $x \sim 340$ m	After the road (Elev. 180-160 m R.L.).
One (?) dropshaft		Elev. 160 m R.L..
Dropshaft cascade (?) : at least three dropshafts	$x \sim 490$ m	Cortijo los N.. Downstream of junction with Veneros branch junction.

References : [Al] ALLAIS (1933); [Ca] CARTON (1899); [Co1] CONSEIL GÉNÉRAL DU RHÔNE (1991); [CQ] COQUET (1966); [Gr] GREWE (1986); [LP] LEVEAU and PAILLET (1976); [Lop] LOPEZ-CUERVO (1985); [PR] PINETTE and REBOURG (1986); [Ve] VERTET (1977); [Vi1] VILLANUEVA (1993); [Vi2] VILLANUEVA (1996).

Notes : d_c : critical flow depth; ΔH : total head loss. Sites names are listed from upstream to downstream (for a given aqueduct branch)

sign was used at a small number of shafts along the Valdepuentes aqueduct (Spa.) : the flow direction turned 90-degrees (Fig. 2B and 3B).

Overall there is little information on the hydraulic performances of dropshaft cascades in Roman aqueducts. In the present study, the hydraulics of Roman dropshafts is re-visited using both physical and analytical models. The results provide a new understanding of the dropshaft cascade operation. The performances are also compared with modern designs. It will be shown that the Roman dropshaft design is an efficient low-head energy dissipator.

Experimental apparatus

Three dropshaft models were studied (Table 2, Fig. 3). The models were built in marine plywood and perspex, with a vertical square dropshaft ($B = L$). The upstream channel was open while the downstream conduit was covered and ended with a free overfall. The discharges were deduced from the brink depth measurements which were first calibrated in-situ with volume-per-time discharge data. [A calibration curve was obtained for each model.] Free-surface elevations were recorded with pointer gauges in the upstream and downstream channels, while the free-surface height in the shaft was measured with rulers. The total head was measured with a total head tube ($\phi = 1$ mm). Additional information were obtained with high-speed photography and video-camera. Further details of the experimental setup are presented in CHANSON (1998).

The upstream and downstream channels operated as free-surface flow for all investigated flow conditions. Indeed water flowed as open channel flow in the Roman aqueducts although the conduit height D ranged from 1 to 2 m for ease of construction and maintenance. The water depths were usually less than 0.2 to 0.3 m at maximum flow rates (e.g. BLACKMAN 1978, HODGE 1992, CHANSON 1998).

Most experiments were conducted with subcritical inflow conditions. A number of tests were performed with supercritical inflows in the model 2 only.

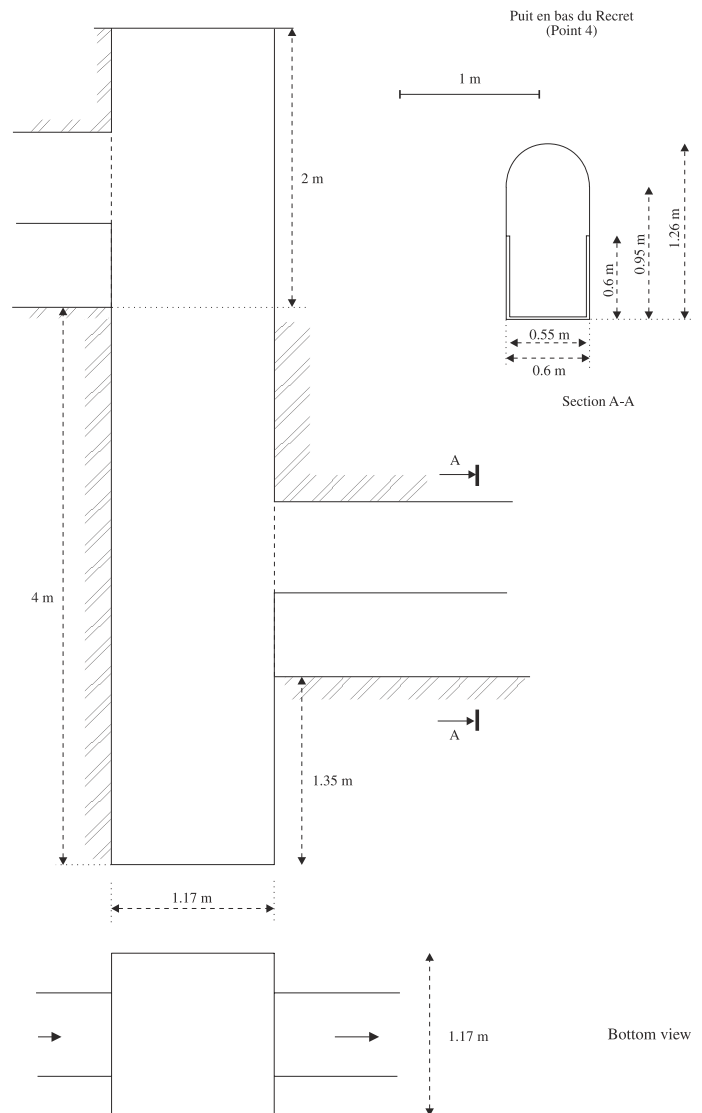


Fig. 2 Well-documented Roman dropshafts. (A) Puit-en-bas, Retret, Yzeron aqueduct, France ($Q_{\max} \sim 0.15$ m³/s)

Table 2: Experimental studies of vertical dropshafts

Study	Upstream conduit	Shaft	Downstream conduit	Flow conditions	Remarks
(1)	(2)	(3)	(4)	(5)	(6)
APELT (1984)	Circular $\phi = 0.152$ m	Square B = L = 0.152 m h = 0.325 m, P = 0	Circular $\phi = 0.152$ m	$0.0022 \leq Q \leq 0.026$ m ³ /s	Energy dissipation downstream of culverts.
	Circular $\phi = 0.152$ m	Square B = L = 0.203 m h = 0.325 m, P = 0	Circular $\phi = 0.152$ m		
RAJARATNAM et al. (1997)	Circular $\phi = 0.154$ m	Vertical plate L = 0.5 m, h = 2.9 m	N/A	$Q \leq 0.042$ m ³ /s	Series 3. Sewer dropshaft models.
	Circular $\phi = 0.154$ m	Circular $\phi = 0.29$ m h = 2.11 m, P = 0	Circular $\phi = 0.29$ m	$0.0021 \leq Q \leq 0.042$ m ³ /s	Series 4.
	Circular $\phi = 0.154$ m	Circular $\phi = 0.29$ m h = 2.11 m, P = 0	Circular $\phi = 0.29$ m	$0.0021 \leq Q \leq 0.042$ m ³ /s	Series 5. Curved inlet radius.
	Circular $\phi = 0.154$ m	Circular $\phi = 0.152$ m, P = 0	Circular $\phi = 0.152$ m	$0.0021 \leq Q \leq 0.042$ m ³ /s	Series 6. Curved inlet radius.
Present Study					
Model 1 (Recret, Puit-en-bas)	Rectangular b = 0.144 m $\theta = 0.17^\circ$	Square B = L = 0.30 m h = 0.505 m P = 0.365 m	Rectangular b = 0.15 m D = 0.25 m $\theta = 0.37^\circ$	$0.0002 \leq Q \leq 0.018$ m ³ /s	Open upstream conduit. 1:4 scale model (Yzeron aqueduct).
Model 2 (Valdepuentes)	Rectangular b = 0.11 m $\theta = 0.17^\circ$	Square B = L = 0.20 m h = 0.688 m P = 0.201 m	Rectangular b = 0.11 m D = 0.21 m	$0.00005 \leq Q \leq 0.019$ m ³ /s (a) Sub-critical inflow (b) Supercritical inflow: $2 \leq Fr \leq 15$	Open upstream conduit. Dimensions scaled upon Valdepuentes dropshaft dimensions.
Model 3 (Valdepuentes, 90-degree bend)	Rectangular b = 0.11 m $\theta = 0.17^\circ$	Square B = L = 0.20 m h = 0.688 m P = 0.201 m	Rectangular b = 0.11 m D = 0.21 m 90-degree bend	$0.00008 \leq Q \leq 0.022$ m ³ /s	Open upstream conduit. 1:4.5 scale model (Valdepuentes aqueduct).

Flow patterns and dropshaft operation

Several flow patterns were observed as functions of the flow rate and dropshaft dimensions. For the models 1 and 2⁴, three flow regimes may occur (Fig. 4). The transition conditions between regimes are summarised in Table 3. The observations (Table 3, column 4) are compared with analytical calculations of the nappe trajectory developed by CHANSON (1998) (Table 3, column 5). At low flow rates, the free-falling nappe impacts into the shaft pool (regime R1, Fig. 3A and 4A). Substantial air bubble entrainment takes place and the entrained air bubbles occupy most of the dropshaft pool. At the lowest flow rates, the free-falling nappe contracts down the jet trajectory until the outer edges intersect (regime R1a). When the side-edges of the jet intersect, a ‘fin’ or ‘central ridge’ develops with a thickness much smaller than the other transverse dimension until nappe impact into the shaft pool. With increasing discharges, the nappe trajectory enlarges, the jet outer edges do not intersect before impingement and no central-ridge formation occurs (regime R1b). In the downstream channel, the flow is supercritical (in absence of downstream backwater effect) and shock waves develop.

4. in the model 3, only the regimes R1 and R3 are observed.

Table 3: Transition between flow regimes (subcritical inflow conditions)

Flow conditions	h/L	h/D	d _c /L Data	d _c /L Theory
(1)	(2)	(3)	(4)	(5)
Transition regime R1 to R2				
Model 1	2.90	3.48	0.15	0.09
Model 2	3.34	3.18	0.10	0.08
Transition regime R2 and R3				
Model 1	2.90	3.48	0.30	0.12
Model 2	3.34	3.18	0.15	0.11

For larger discharges, the upper nappe of the free-falling jet impacts into the downstream channel, flowing in between the inlet invert and obvert (regime R2). The pool free-surface level increases significantly, and lesser air bubble entrainment is observed in the pool. High risks of scour exist at the obvert edge and on the invert of the downstream channel (Fig. 4B). The jet impact onto the downstream channel is further associated with the development of sidewall standing waves in the conduit, similar to those observed by CHANSON and TOOMBES (1998).

At large flow rates, the free-jet impacts onto the opposite wall above the downstream conduit obvert (regime R3) (Fig. 3B and 4C). Significant water deflections take place in the shaft. During the study, the impact angle of the nappe onto the wall was shal-

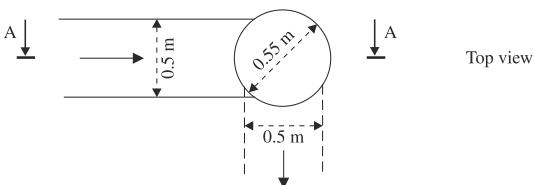
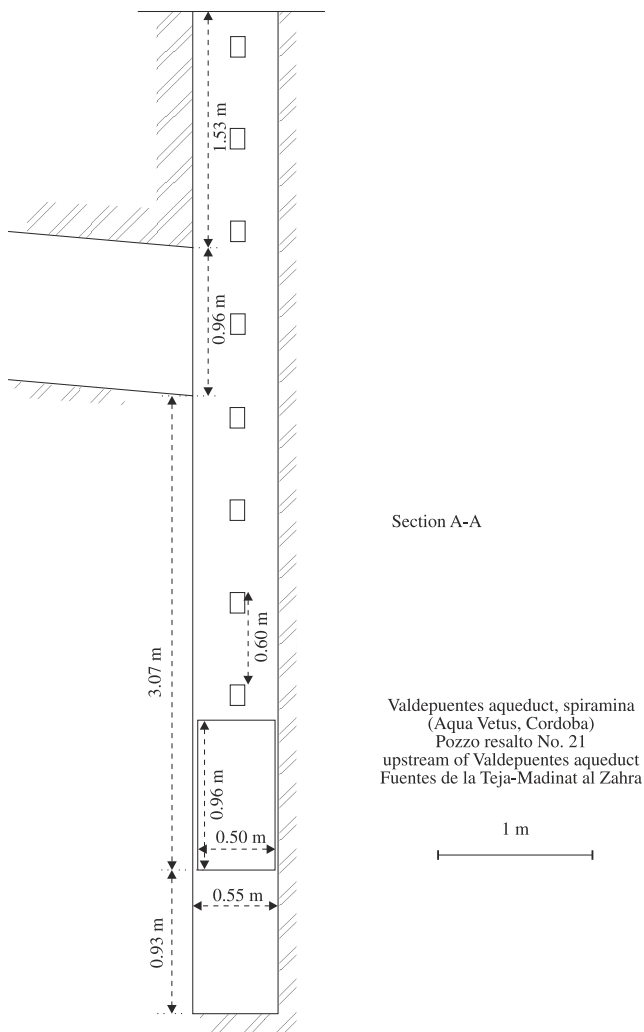


Fig. 2 Well-documented Roman dropshafts. (B) Pozzo resalto No. 21, Valdepuentes aqueduct, Spain ($Q_{\max} \sim 0.255 \text{ m}^3/\text{s}$). Fuentes de la Teja-Madinat al Zahra, upstream of Valdepuentes bridge

low and did not produce a formed roller as observed by RAJARATNAM et al. (1997).

For all the experiments, the flow in the downstream conduit was found to leave the dropshaft as a supercritical open channel flow. A similar observation was noted by RAJARATNAM et al. (1997).

Flow properties

Pool free-surface height data are reported in Figure 5A where y_p is the free-surface height above downstream invert (Fig. 4A). The pool height rises with increasing discharges up to about $y_p/D \sim 1$ to 1.2, then remains stable with larger flow rates, until it rises again for $Q' \geq 1.2$, where $Q' = Q/\sqrt{g \cdot b^2 \cdot D^3}$ and $Q' = Q/\sqrt{g \cdot \pi^2 \cdot D^5/16}$



Fig. 3 Photographs of the physical models. (A) Photograph of the model 1 (Regime R1, $Q = 0.001 \text{ m}^3/\text{s}$) (high-speed photograph)

for rectangular and circular conduits respectively, D is the downstream conduit height, Q is the flow rate, and b is the upstream channel width (Fig. 4A). The results are consistent with the observations of APELT (1984) and RAJARATNAM et al. (1997) (Table 1, Fig. 5A).

The dimensionless bubble penetration depth is plotted in Figure 5B as a function of the dimensionless flow rate d_c/h where d_c is the critical depth in the upstream channel and h is the drop in invert elevation. In flow regimes R1 and R3, substantial flow aeration takes place, the bubbles plunge deep down to the shaft bottom and the bubble cloud occupies more than half of the shaft pool volume (e.g. Fig. 3). The entrained bubbles enhance the air-water interface area and the air-water gas transfer: i.e., re-aeration. The flow regime R2 is less efficient in entraining air because the nappe interacts with the downstream conduit inlet. The entrained bubbles do not have enough downward momentum to reach the shaft bottom.

Residual energy data are presented in Figure 5C. The data are presented as H_{res}/H_1 as a function of the dimensionless flow rate d_c/h (or $\sqrt[3]{Q^2/(g \cdot D^2)}/h$ for circular pipes), where H_{res} is the residual head in the downstream channel and H_1 is the upstream total head measured above the downstream channel invert. The results are compared with the data of RAJARATNAM et al. (1997). Low

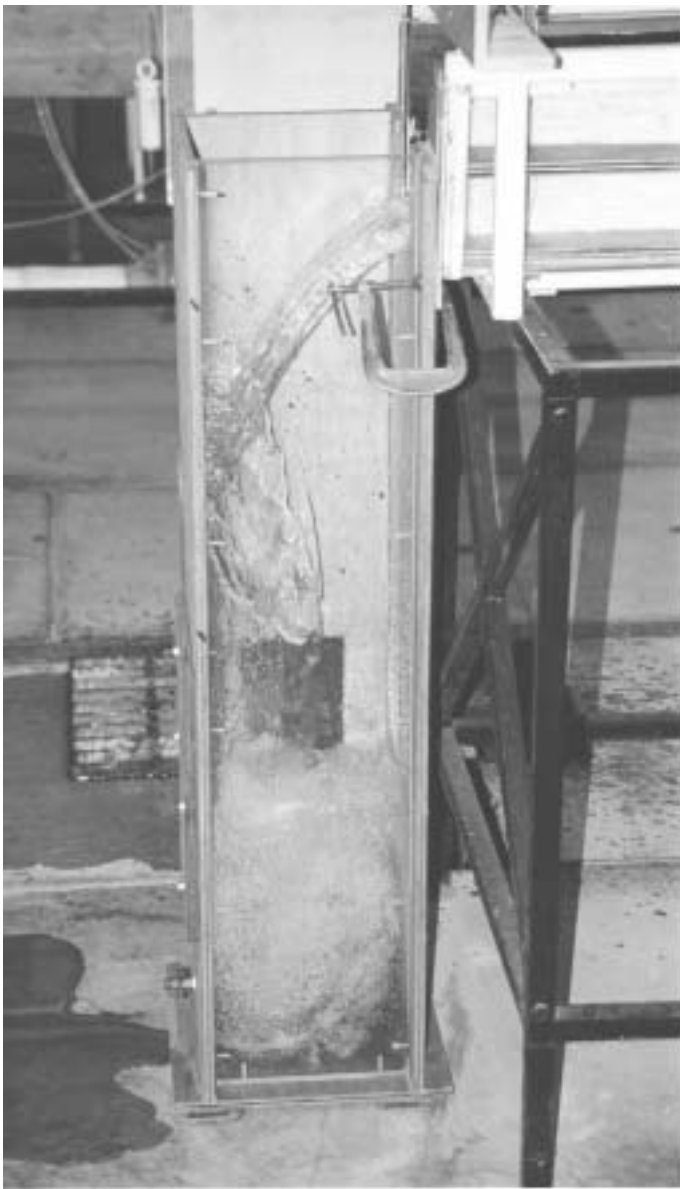


Fig. 3 Photographs of the physical models. (B) Photograph of the model 3 (Regime R3, $Q = 0.004 \text{ m}^3/\text{s}$)

residual heads, associated with high energy dissipation, are achieved at low flow rates (Regime R1) (Fig. 5C). Poor dissipation performances are observed in regime R2. In regime R3, the dimensionless residual head ranges from 20 to 55% depending upon the model geometry.

A comparison between the three model performances suggests that the model 3 is a more efficient dissipator (Fig. 5C). A dominant feature of this design (Fig. 3) is the absence of the flow regime R2 characterised by lesser energy dissipation and some risks of scour. In regime R1, the performances of the three models are very close (Fig. 5).

Discussion

Compared with modern designs, Roman dropshafts exhibited an unusual shape : i.e., a deep wide shaft pool. Modern dropshafts do not include a pool, the shaft bottom being at the same elevation

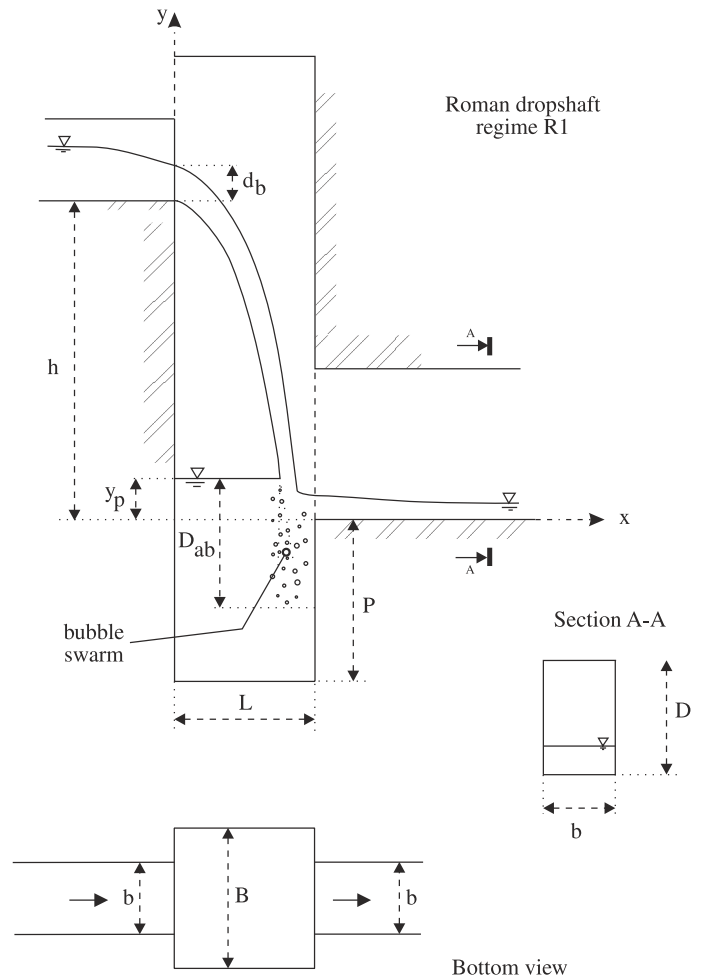


Fig. 4 Basic flow patterns, including notation. (A) Regime R1.

Regime R2

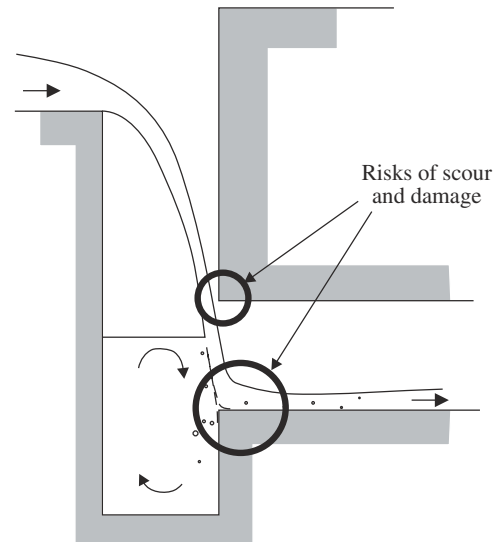


Fig. 4 Basic flow patterns, including notation. (B) Regime R2

as the downstream channel bed to minimise construction costs. In Roman dropshafts, the pool of water acts as a cushion at nappe impact, preventing scour at the shaft bottom. The shaft pool facilitates further the entrainment (by plunging jet) of air bubbles deep

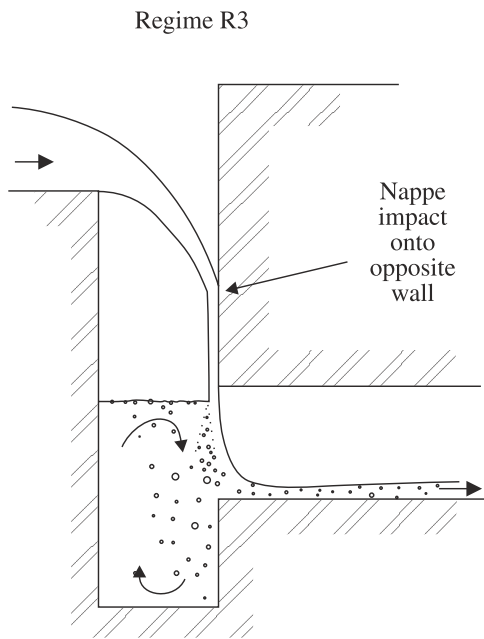


Fig. 4 Basic flow patterns, including notation. (C) Regime R3

down, maximising the bubble residence time and hence the air-water gas transfer. The design contributes successfully to an enhancement of the DO content (dissolved oxygen content). Roman dropshafts had a wider shaft (i.e. $B/b > 2$) than modern designs (i.e. $B/b = 1$ to 1.5). It is believed that the wider shaft was selected for an easier construction and maintenance (e.g. Conseil Général du Rhône 1996).

The rate of energy dissipation of Roman dropshaft is compared with the performances of modern drop structures and vortex dropshafts in Figure 6. The calculations for drop structures and vortex dropshafts were based upon the works of RAND (1955) and VISCHER and HAGER (1995) respectively. The results (Fig. 6) suggest that Roman dropshafts operating at low flow rates (i.e. regime R1) were very efficient energy dissipators by modern standards. Today the Roman dropshaft design may be considered as a low-head low-discharge dissipator.

The experimental investigation has highlighted that the best per-

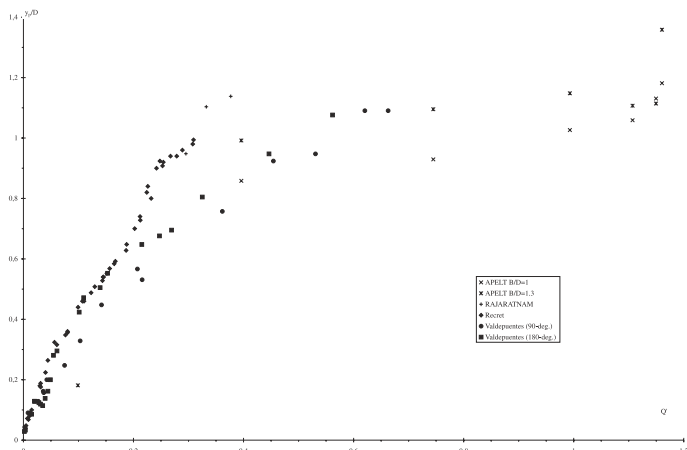


Fig. 5 Hydraulic performances of the dropshaft models. (A) Dimensionless shaft pool free-surface height y_p/D

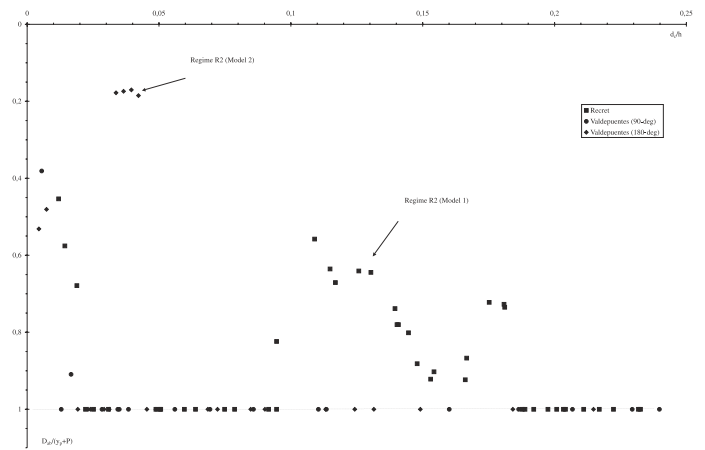


Fig. 5 Hydraulic performances of the dropshaft models. (B) Dimensionless bubble swarm depth $D_{ab}/(y_p+P)$

formances of the Roman dropshaft design are achieved with a flow regime R1. The study shows also that the flow regime R2 is associated with high risks of scour and erosion at the lower conduit inlet and obvert. The Roman aqueducts had to be designed with dropshafts operating in a flow regime R1 for long-lasting operation. Based on analytical calculations of the nappe trajectory and impact conditions, the optimum operation (i.e. regime R1) of Roman dropshafts operating with subcritical inflow must satisfy:

$$Q < 0.1292 * \sqrt{g} * b * \frac{L^3}{h^{3/2}} \quad \text{Regime R1 (1)}$$

where b is the dropshaft inflow width, L is the shaft length and h is the invert drop (Fig. 4A) (CHANSON 1998). For dropshafts operating with supercritical inflow, the inflow conditions must satisfy :

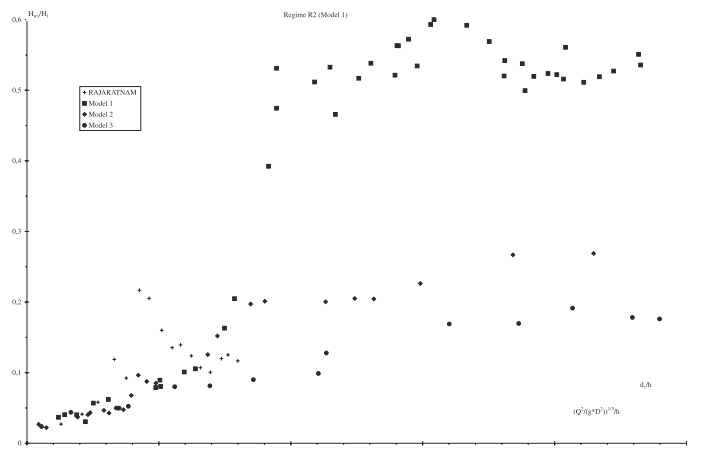


Fig. 5 Hydraulic performances of the dropshaft models. (C) Dimensionless residual head H_{res3}/H_1 as a function of the dimensionless flow rate d_c/h (or $\sqrt[3]{Q^2/(g*D^2)}/h$ for circular pipes)

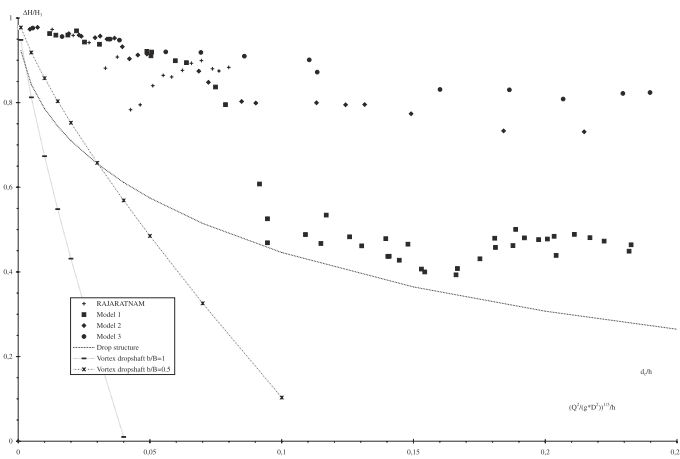


Fig. 6 Rate of energy dissipation $\Delta H/H_1$ as a function of the ratio d_c/h (or $\sqrt[3]{Q^2/(g \cdot D^2)}/h$ for circular pipes). Comparison between Roman dropshaft model (Present study) and modern drop structures : drop structures (RAND 1955) and vortex dropshaft (VISCHER and HAGER 1995)

$$\frac{V_b}{\sqrt{g \cdot L}} < \frac{1}{2} \cdot \frac{h}{L} *$$

$$\left(\sqrt{8 \cdot \frac{L}{h} + \frac{Q^2}{g \cdot b^2 \cdot h^2 \cdot L}} - \frac{Q}{\sqrt{g \cdot b^2 \cdot h^2 \cdot L}} \right)$$

Regime R1 (2)

where V_b is the inflow velocity.

Operation of dropshaft cascade

A dropshaft cascade (Fig. 1) is basically a high-head dissipator. For example, $\Delta H = 200$ m at Madinat-al-Zhara, Valdepuentes aqueduct. History showed that this design could operate successfully for long periods and required (likely) little maintenance. For example, the Valdepuentes aqueduct and its dropshaft cascades were used by the Romans and later re-used by the Muslims : their operation lasted for several centuries (VILLANUEVA 1993, 1996). Of interest the model 3 design (with a 90-degree bend) may provide a very-compact dissipation structure if the dropshafts are installed in a (square) spiral disposition.

The operation of the dropshaft cascades is not only a function of the dropshaft performances (see above) but it is also related to the connecting conduit geometry. At Recret (Yzeron aqueduct), the conduits had a mild slope ($\theta \approx 0.1$ to 0.6°), and a hydraulic jump took place between dropshafts, as sketched in Figure 1. Similarly the connecting conduits had a mild slope at Montjeu (Brisecou forest), Cuicul and Köln aqueducts. At Cerro de los Pinos (Valdepuentes aqueduct), the channel slope was steep (about 2.9°) leading to a supercritical flow in the conduits. The effect of a supercritical inflow was investigated in the model 2. The results showed that the inflow conditions affected the type of flow regime particularly at low flow rates (e.g. Eq. (1) and (2)). However, for a given flow regime, the inflow Froude number had little if no effect on the rate of energy dissipation, shaft aeration and pool level. [Slightly better energy dissipation was observed with supercritical inflows with $Fr > 10$ in regime R3.]

Conclusion

Roman engineers built dams, spillways and hydraulic structures all around the Mediterranean sea. Some aqueducts were equipped with dropshafts and dropshaft cascades (Table 1). The hydraulics of Roman dropshaft was investigated using laboratory models. The results are compared with an analytical model.

Three flow regimes were observed basically. Optimum dropshaft operation occurred in the flow regime R1, characterised by low flows and nappe impact into the shaft pool. The dropshaft operation was more efficient in terms of energy dissipation and air bubble entrainment than modern designs (Fig. 6). For intermediate flow rates, unfavourable flow conditions may occur (regime R2). At large discharges, the operation of Roman dropshaft is similar to that of modern structures.

The issues of re-aeration should also be considered. Most aqueducts were covered along their entire length, limiting the gas transfer at the free-surface and the downstream waters were low in dissolved oxygen (DO) content, unless re-oxygenation devices were installed. The writer suggests that dropshafts might have been introduced, in place of steep chutes, to enhance the water quality and to re-oxygenate the water.

Acknowledgments

The writer wishes to acknowledge the following people (in alphabetical order) for their help and assistance : Professor C. Apelt, The University of Queensland, Australia; Dr D. Blackman, Monash University, Australia; Ms Chou Y.H., Brisbane, Australia; Dr M.R. Gourlay, The University of Queensland, Australia; Dr A.T. Hodge, Carleton University, Canada; Mr G. Illidge, The University of Queensland, Australia; Mr P. Leveau, Université d'Aix-en-Provence, France; Professor N. Rajaratnam, University of Alberta, Canada; Dr A.V. Villanueva, University of Cordoba, Spain.

References/bibliographie

- ALLAIS, Y. (1933). "L'Alimentation en Eau d'une Ville Romaine d'Afrique : Cuicul (Djemila)," ('The water Supply of a Roman City in Africa : Cuicul (Djemila).') *5th Congrès International d'Archéologie*, Alger, pp. 93-117 (in French).
- APELT, C.J. (1984). "Goonyella Railway Duplication Drop Structures and Energy Dissipators at Culvert Outlets. Model Studies." *Report CH27/84*, Dept. of Civil Engineering, University of Queensland, Australia, Feb., 10 pages, 11 figures & 37 plates.
- ASHBY, T. (1935). "The Aqueducts of Ancient Rome." *Clarendon Press*, Oxford, UK, edited by I.A. RICHMOND, 342 pages.
- BLACKMAN, D.R. (1978). "The Volume of Water Delivered by the Four Great Aqueducts of Rome." *Papers of the British School at Rome*, Vol. 46, pp. 52-72.
- CARTON (1899). "Notices sur les Fouilles Exécutées à Dougga." *Bulletin Trimestriel de Géographie et d'Archéologie de la S.G.A.P.O.*, Vol. 13, pp. 157-159 (in French).

- CHANSON, H. (1995). "Hydraulic Design of Stepped Cascades, Channels, Weirs and Spillways." *Pergamon*, Oxford, UK, Jan., 292 pages.
- CHANSON, H. (1997). "A Short History of Stepped Cascades in Australia." *ANCOLD Bulletin*, No. 106, Aug., pp. 101-111.
- CHANSON, H. (1998). "The Hydraulics of Roman Aqueducts : Steep Chutes, Cascades and Dropshafts." *Research Report No. CE156*, Dept. of Civil Engineering, University of Queensland, Australia (ISBN 0 86776 775 3).
- CHANSON, H. (2000). "Hydraulics of Roman Aqueducts : Steep Chutes, Cascades and Dropshafts." *American JI of Archaeology*, Vol. 104, No. 1, Jan., pp. 47-72.
- CHANSON, H., and TOOMBES, L. (1998). "Supercritical Flow at an Abrupt Drop : Flow Patterns and Aeration." *Can. JI of Civil Eng.*, Vol. 25, No. 5, Oct., pp. 956-966.
- CONSEIL GÉNÉRAL DU RHÔNE (1991). "Préinventaire des Monuments et Richesses Artistiques. II L'Aqueduc Romain de l'Yzeron." ('Pre-inventory of the Monuments and Art Treasures. II The Roman Aqueduct of the Yzeron.') *Bosc Frères Publ.*, Lyon, France, Henri HOURS Editor, 168 pages & 1 Map (in French).
- CONSEIL GÉNÉRAL DU RHÔNE (1996). "Préinventaire des Monuments et Richesses Artistiques. IV Lyon. L'Aqueduc Romain du Gier." ('Pre-inventory of the Monuments and Art Treasures. IV Lyon. The Roman Aqueduct of the Gier.') *Bosc Frères Publ.*, Lyon, France, Jean BURDY Editor, 407 pages & 1 Map (in French).
- COQUET, M. (1966). "Les Aqueducs Romains de Beaulieu et les Puits de Rupture de pente." ('The Roman Aqueducts of Beaulieu and the Stepped Cascades.') *Cahiers Ligures de Préhistoire et d'Archéologie*, Vol. 15, pp. 283-295 (in French).
- ERVINE, D.A., and AHMED, A.A. (1982). "A Scaling Relationship for a Two-Dimensional Vertical Dropshaft." *Proc. Intl. Conf. on Hydraulic Modelling of Civil Engineering Structures*, BHRA Fluid Eng., Coventry, UK, paper E1, pp. 195-214.
- FEVRIER, P.A. (1979). "L'Armée Romaine et la Construction des Aqueducs." ('The Roman Army and the Construction of Aqueducts.') *Dossiers de l'Archéologie*, Séries Les Aqueducs Romains, Vol. 38, Oct./Nov., pp. 88-93 (in French).
- GREWE, K. (1986). "Atlas der Römischen Wasserleitungen nach Köln." ('Atlas of the Roman Hydraulic Works near Köln.') *Rheinland Verlag*, Pulheim, Germany (in German).
- HODGE, A.T. (1992). "Roman Aqueducts & Water Supply." *Duckworth*, London, UK, 504 pages.
- JAIN, S.C., and KENNEDY, J.F. (1983). "Vortex-Flow Drop Structures for the Milwaukee Metropolitan Sewerage District Inline Storage." *IJHR Report No. 264*, Iowa Inst. of Hyd. Res., University of Iowa, USA..
- LEVEAU, P. (1991). "Research on Roman Aqueducts in the past Ten Years." *Future Currents in Aqueduct Studies*, Leeds, UK, T. HODGE ed., pp. 149-162.
- LEVEAU, P., and PAILLET, J.L. (1976). "L'Alimentation en Eau de Caesarea de Maurétanie et l'Aqueduc de Charchell." ('The Water Supply of Caesarea of Mauretanie and the Charchell Aqueduct.') *Librairie Edition L'Harmattan*, Paris, France, 183 pages & 10 plates (in French).
- LOPEZ-CUERVO, S. (1985). "Medina Az-Zahra Ingeniera y Formas." *Publicaciones del Ministerio de Obras Publicas y Urbanismo*, Madrid, Spain 169 pages (in Spanish).
- PINETTE, M., and REBOURG, A. (1986). "Autun (Saône-et-Loire) Ville Gallo-Romaine." *Guides Archéologiques de la France*, Imprimerie Nationale, Ministère de la Culture et de la Communication, France (In French).
- RAJARATNAM, N., MAINALI, A., and HSUNG, C.Y. (1997). "Observations on Flow in Vertical Dropshafts in Urban Drainage Systems." *Jl of Environmental Engrg.*, ASCE, Vol. 123, No. 5, pp. 486-491.
- RAKOB, F. (1974). "Das Quellenheigtum in Zaghouan und die Römische Wasserleitung nach Karthago." *Mitt. des Deutschen Archäologischen Instituts Roemische Abteilung*, Vol. 81, pp. 41-89, Plates 21-76 & Maps (in German).
- RAND, W. (1955). "Flow Geometry at Straight Drop Spillways." *Proceedings*, ASCE, Vol. 81, No. 791, Sept., pp. 1-13.
- VERTET, H. (1977). "Observations sur les Aqueducs de Rusicade (Algérie)." ('Observations on the Aqueducts of Rusicade (Algérie).') *Journées d'Etude sur les Aqueducs Romains*, Lyon, France, 26-28 Mai (also *Les Belles Lettres Publ.*, Paris, France, 1983, pp. 349-369) (in French).
- VILLANUEVA, A.V. (1993). "El Abastecimiento de Agua a la Cordoba Romana. I : El Acueducto de Valdepuentes." ('The Water Supply of the Roman Cordoba. I : Aqueduct of Valdepuentes.') *Monografias No. 197*, Universidad de Cordoba, Servicio de Publicaciones, Cordoba, Spain, 172 pages (in Spanish).
- VILLANUEVA, A.V. (1996). "El Abastecimiento de Agua a la Cordoba Romana. II : Acueductos, Ciclo de Distribución y Urbanismo." ('The Water Supply of the Roman Cordoba. II : Aqueduct, Distribution System and Urbanism.') *Monografias No. 251*, Universidad de Cordoba, Servicio de Publicaciones, Cordoba, Spain, 222 pages (in Spanish).
- VISCHER, D., and HAGER, W.H. (1995). "Energy Dissipators." *IAHR Hydraulic Structures Design Manual No. 9*, Hydraulic Design Considerations, Balkema Publ., Rotterdam, The Netherlands, 201 pages.

Notation

B	dropshaft width (m);
b	open channel width (m);
C_d	drag coefficient;
D	1- conduit diameter (m); 2- conduit height (m);
D_{ab}	bubble penetration depth (m) measured vertically from the free-surface;
d	flow depth (m) measured perpendicular to the channel bed;
d_c	critical flow depth (m); in a rectangular channel: $d_c = \sqrt[3]{q^2/g}$;
Fr	Froude number; for a rectangular channel: $Fr = V/\sqrt{g*d} = Q/\sqrt{g*d^3*b^2}$;
g	gravity constant (m/s ²);

H	total head (m);
H_{res}	residual head (m) : $H_{res} = H_1 - \Delta H$;
H_1	upstream total head (m);
h	invert drop (m) at a vertical dropshaft;
L	dropshaft length (m);
P	(shaft) pool height (m), measured from the shaft bottom to the downstream conduit invert;
Q	total volume discharge (m^3/s) of water;
Q_{max}	maximum flow rate (m^3/s) of the aqueduct;
Q'	dimensionless discharge number; $1-Q' = Q/\sqrt{g*b^2*D^3}$ for rectangular channels; $2-Q' = Q/\sqrt{g*\pi^2*D^5/16}$ for circular conduits;
q	discharge per meter width (m^2/s); for a rectangular channel : $q = Q/b$;
V	flow velocity (m/s);

V_b	brink flow velocity (m/s);
x	horizontal distance (m);
y_p	free-surface height (m) in a shaft pool above the downstream conduit invert;

Greek symbols

ΔH	head loss (m) : i.e., change in total head;
π	$\pi = 3.141592653589793238462643$;
θ	bed (invert) slope;
ϕ	diameter (m);

Abbreviations

R1	flow regime R1 (Fig. 4A);
R2	flow regime R2 (Fig. 4B);
R3	flow regime R3 (Fig. 4C).